

## THREE Co(II), Ni(II) AND Cu(II) SCHIFF BASE COMPLEXES INCORPORATING 2-[(4-((4-METHYLPHENYL)SULFONOTHIOYL)OXY)PHENYL)METHYLENE]AMINO}BENZOIC ACID: SYNTHESIS, STRUCTURAL, DFT, BIOLOGICAL AND MOLECULAR DOCKING INVESTIGATION

Wassila Derafa<sup>1</sup>, Nadia A.A. Elkanzi<sup>1\*</sup>, Ali M. Ali<sup>2</sup> and Aly Abdou<sup>2</sup>

<sup>1</sup>Chemistry Department, College of Science, Jouf University, Sakaka, 2014, Saudi Arabia

<sup>2</sup>Chemistry Department, Faculty of Science, Sohag University, Sohag 82524, Egypt

(Received September 26, 2023; Revised November 14, 2023; Accepted November 15, 2023)

**ABSTRACT.** New 2-[(4-((4-methylphenyl)sulfonothioyl)methylene)aminobenzoic acid ligand-Co(II), Ni(II), and Cu(II) complexes are synthesized and characterized in this article. Elemental analysis, mass spectroscopy, conductivity tests, magnetic susceptibility, Fourier transform infrared spectroscopy, thermogravimetric analysis, electronic absorption spectroscopy, and density functional theory calculations were used to determine the coordination mode, and geometry of the synthesized compounds. The Schiff-base ligand was shown to be mono-negatively charged and coordinate to metal ions in a bi-dentate mode through azomethine nitrogen (-CH=N-) and carboxylic Oxygen (-COOH). Density functional theory (DFT) calculations were performed in addition to the experimental data to assess the most probable structures of the complexes. In addition, the biological activities of these compounds were evaluated by *in vitro* antibacterial and antifungal assays. These novel Co(II), Ni(II), and Cu(II) compounds were shown to be active against a wide variety of microorganisms, including Gram-positive and Gram-negative bacteria, as well as fungi. Following that, molecular docking was used to analyze the complexes' interactions with bacterial proteins, validating the therapeutic potential of the metal-containing compounds.

**KEY WORDS:** Metal complexes, Schiff-base, DFT, Antibacterial, Antifungal, Molecular docking

### INTRODUCTION

Schiff-bases and their metal complexes are versatile compounds that have attracted considerable attention in various fields of chemistry, biology, and medicine. They are formed by the condensation of a carbonyl compound, such as an aldehyde or a ketone, with a primary amine, resulting in the formation of an imine or azomethine group (>C=N-) [1]. Schiff-bases can act as ligands that coordinate to different metal ions, forming stable and diverse metal complexes with various geometries and properties.

Schiff-bases derived from anthranilic acid are a special class of Schiff-bases that have the 2-aminobenzoic acid moiety in their structure. Anthranilic acid is an important intermediate in the biosynthesis of tryptophan and other indole derivatives [2]. It can also act as a precursor for the synthesis of various heterocyclic compounds, such as quinolines, benzoxazoles, benzimidazoles, and benzothiazoles [3]. Schiff-bases derived from anthranilic acid can be obtained by the condensation of anthranilic acid or its derivatives with various aldehydes or ketones, such as salicylaldehyde, acetylacetone, benzil, and 2,3-pentanedione [4].

Schiff-bases derived from anthranilic acid and their metal complexes have been extensively studied for their diverse applications in different fields of science and technology. Some of the important applications are: They can be used as ligands for the synthesis of novel coordination polymers and metal-organic frameworks (MOFs) with potential applications in gas storage, separation, catalysis, and luminescence [5]. They can exhibit fluorescence and phosphorescence properties that make them suitable for the fabrication of organic light-emitting diodes (OLEDs), chemosensors, biosensors, and bioimaging agents [6]. They can show anticancer, antibacterial,

\*Corresponding author. E-mail: [kanzi20@yahoo.com](mailto:kanzi20@yahoo.com) ; [nahasan@ju.edu.sa](mailto:nahasan@ju.edu.sa)

This work is licensed under the Creative Commons Attribution 4.0 International License

antifungal, antiviral, antimalarial, antitubercular, anti-inflammatory, and antioxidant activities that make them potential candidates for drug design and development [7]. They can act as corrosion inhibitors for various metals and alloys in different acidic and alkaline media. They can serve as analytical reagents for the spectrophotometric determination of various metal ions, such as copper, iron, nickel, cobalt, zinc, and manganese. Therefore, Schiff-bases derived from anthranilic acid and their metal complexes are important and useful compounds that have a wide range of applications in various fields of science and technology.

On the other hand, Sulfonate compounds are organic molecules that contain the functional group  $R-S(=O)_2-O-$ , where R is an organic group [8, 9]. They can be classified into sulfonate salts and sulfonate esters, depending on the nature of the group attached to the oxygen atom. Sulfonate compounds have a wide range of applications in various fields of chemistry, biology, and medicine, due to their stability, solubility, and reactivity [10, 11]. One of the important applications of sulfonate compounds is their ability to act as ligands for metal ions, forming sulfonate metal complexes [12, 13]. These complexes have diverse structures, properties, and functions, depending on the type of metal ion, the number and geometry of the ligands, and the presence of other coordinating groups. Sulfonate metal complexes have been extensively studied for their potential uses in catalysis, luminescence, sensing, optoelectronics, drug design, and corrosion inhibition.

The aim of this research article is to explore the coordination chemistry of novel Schiff-base ligands derived from 4-tosyl chloride and anthranilic acid, which have not been reported in the literature before. We synthesized and characterized a series of new Co(II), Ni(II), and Cu(II) complexes with these ligands, and investigated their antibacterial and antifungal activities against various microorganisms. We also performed density functional theory (DFT) calculations and molecular docking studies to understand the structural and electronic properties of the ligands and complexes, as well as their possible binding modes with microbial enzymes. This study provides new insights into the synthesis, structure, and biological applications of Schiff-base metal complexes derived from anthranilic acid.

## EXPERIMENTAL

### *Materials*

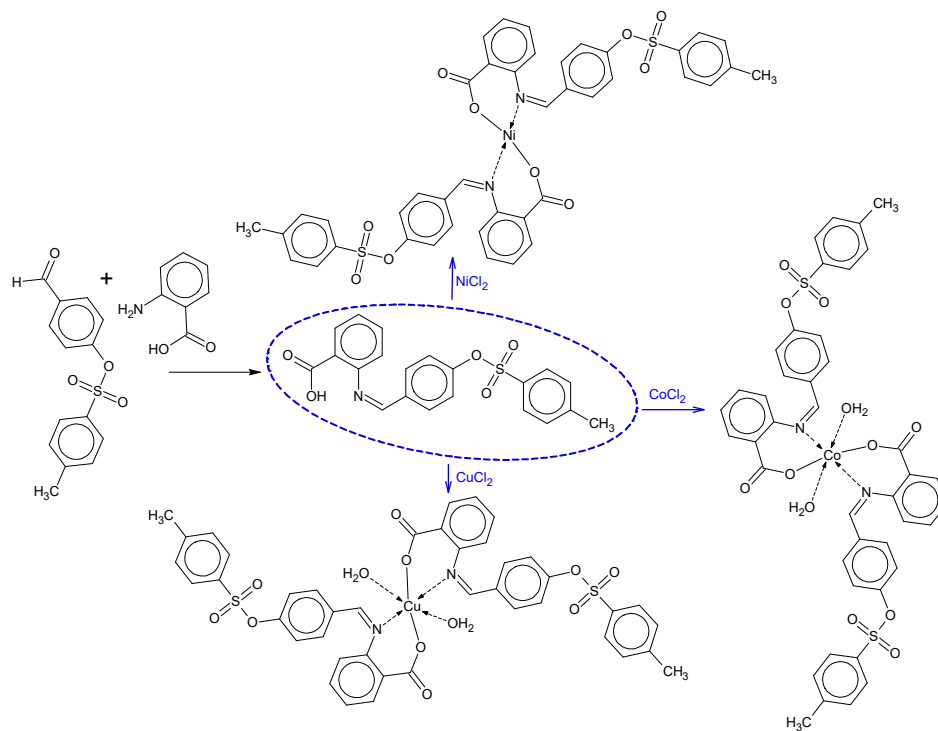
All of the chemicals utilized in the study, such as  $CoCl_2$ ,  $NiCl_2$ , and  $CuCl_2$ , were of reagent quality and were used straight from the chemical companies from whence they were bought. Every one of the solvents was of spectroscopic quality. DMF, DMSO, and acetonitrile were among the solvents used.

### *Synthesis of the Schiff-bases ligand (HL)*

After 10 minutes of stirring a mixture of 4-formylphenyl-4-methylbenzenesulfonate (1 mmol, 2.76 g) and anthranilic acid (1 mmol, 1.37 g), the corresponding Schiff base was produced. After the solid precipitate formed, it was filtered, washed with ethanol solutions of decreasing concentration, air-dried, and crystallized.

### *Synthesis of the metal complexes*

The metal complexes were prepared by dissolving the ligand (1.5 mmol) in hot ethanol (20 mL) and then adding 1.5 mmol each of  $CoCl_2$ ,  $NiCl_2$ , and  $CuCl_2$  in water (20 mL). The process was executed at a comfortable temperature of about 80 degrees Celsius. The solution was refluxed in a water bath with continual magnetic stirring and a nitrogen atmosphere for eight hours. The last step in this process was to dry the product after it had been filtered and washed many times with ethanol.



Scheme 1. Preparation of Schiff-base ligand and its metal complexes.

#### Characterization

The compositions of the complexes were determined using elemental analysis (for C, H, and N content), molar conductance ( $10^{-3}$  mol/L), thermal decomposition (TGA), magnetic measurements, infrared (IR) spectroscopy, and electronic spectra ( $10^{-3}$  mol/L). Elemental analysis was performed at the University of Cairo's Central Laboratory using a Perkin-Elmer 2408 analyzer. Near infrared spectra of KBr pellets were obtained using a Shimadzu DR-8001 spectrometer and an infrared spectrometer. <sup>1</sup>H-NMR spectra of DMSO-d<sub>6</sub> were obtained using a Bruker DRX 400 MHz instrument with TMS as a reference. UV-Vis spectra were obtained using a Jenway UV-Vis spectrophotometer. Thermal decomposition (TGA) analysis was performed on the required compounds using a Shimadzu type 60 H analyzer. The molar conductance of a DMF solution ( $10^{-3}$  mol/L) was measured using a JENWAY model 4320 electronic conductivity meter. The molar magnetic susceptibility of powdered materials was determined using a Bartington Susceptibility machine (model 4320). The stoichiometry of the compounds was determined using a continuous-variation spectrophotometric method.

#### DFT studies

Theoretical simulations have been used in the process of verifying the structure of newly synthesized substances. Gaussian 09w [14] was utilized to do computational research. Density

functional theory (DFT) was conducted using B3LYP method [15, 16] using 6-311G (d,p) [17, 18] basis set for H, C, N, S and O-atoms and LANL2DZ basis set [19] for metal-atom (Co/Ni/Cu).

#### *In vitro* antibacterial and antifungal activity screening

Using the disc diffusion method, we investigated the antibacterial and antifungal characteristics of the free ligand and its metal complexes [20, 21]. Some of the bacteria and fungi were *B. cereus* (+ve), *S. aureus* (+ve), *P. aeruginosa* (-ve), and *E. coli* (-ve). In addition to that, *A. flavus*, *T. rubrum* and *C. albicans* fungi were used. DMSO (dimethylene sulfoxide) was utilized to dissolve the chemicals for solution preparation.

Assaying the free ligand and its complexes for *in vitro* antibacterial and antifungal activity, we employed the disc diffusion method. This experiment was performed on a petri dish. The study's major focus was on eliminating potentially harmful bacteria and fungi. Petri plates were prepared with nutritional agar, and the organisms of interest were seeded into them. Discs 5 mm in diameter and 100 ppm in concentration of the ligand and the metal complexes were distributed uniformly throughout the culture plates. The dishes were then baked for another 24 hours at 37 degrees Celsius. To ascertain whether or not the medicine is antibacterial, inhibition zone (IZ) diameter was.

Chloramphenicol, a popular conventional antibiotic, was shown to be antibacterial and antifungal when used at the same doses and in the same solvent. The activity indices were converted to percentages using the following method so that the antibacterial and antifungal efficacies of the compounds could be compared to a standard. To calculate the percentage of activity (%) between the test material and the reference material,  $\% = (IZ_{\text{test}}/IZ_{\text{Reference}}) \times 100$  [22, 23]. Where;  $IZ_{\text{test}}$  is inhibition zone of the test Material, and  $IZ_{\text{Reference}}$  is inhibition zone of the Reference Material.

#### *Molecular docking studies*

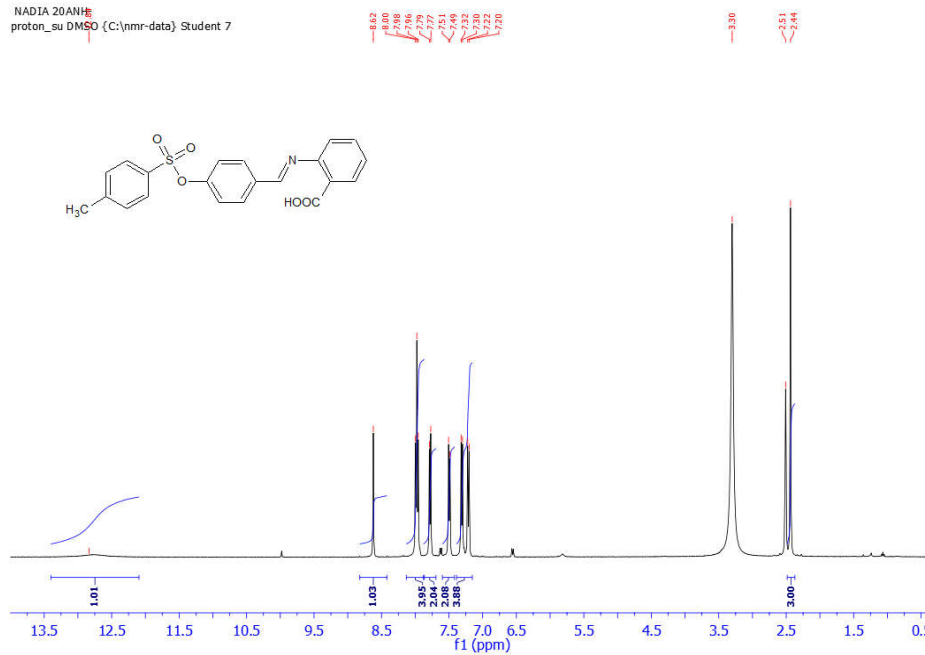
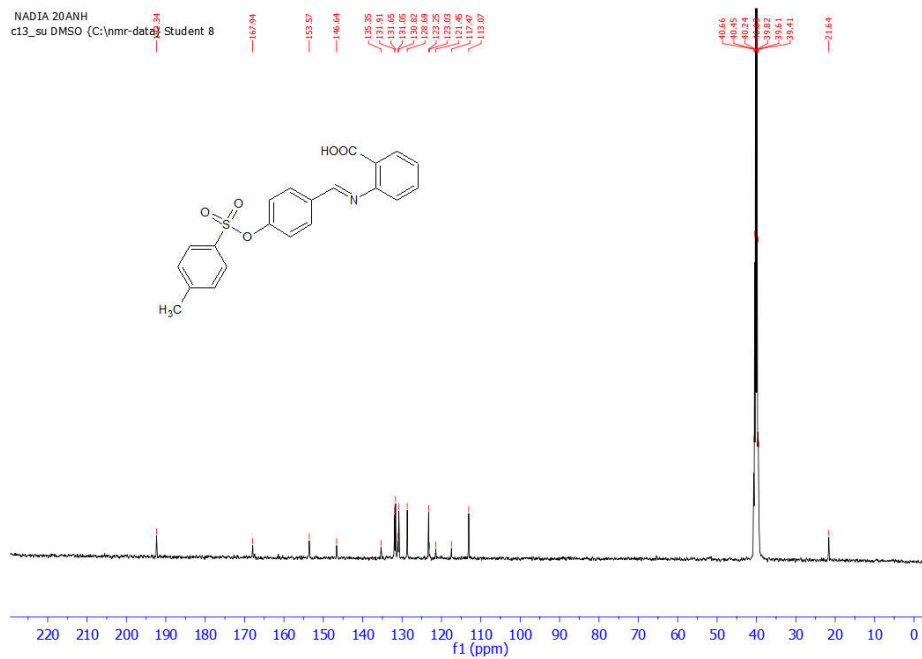
The binding mechanism and ligand-DHPS (dihydropteroate synthase) interactions were theorized by molecular docking experiments. Essential for prokaryotes is the existence of this enzyme, which allows them to produce folic acid. Since practically all bacterial species need folic acid for nucleic acid synthesis [24, 25], it makes for a suitable antibiotic target. Crystal structures of DHPS from *E. coli* and *S. aureus* were utilized as receptors in molecular docking simulations [26, 27], after accessing the RCSB protein data repository. The corresponding PDB identifiers are 5JQ9 and 6CLV.

## RESULTS AND DISCUSSION

#### *Structural characterization of the HL-ligand*

A high yield of the HL ligand was achieved during synthesis (Table 1). Scheme 1 details the steps required to synthesize HL.

FTIR,  $^1\text{H-NMR}$ ,  $^{13}\text{C-NMR}$ , and chemical investigations all corroborated the ligand's structure. In the IR spectra, the (-CH=N) band is located at  $1670\text{ cm}^{-1}$ , while the OH group stretching vibration is located at  $3322\text{ cm}^{-1}$ . The frequencies of  $1581\text{ cm}^{-1}$  for  $\nu_{\text{as}}(\text{COO}^-)$  and  $1424\text{ cm}^{-1}$  for  $\nu_{\text{s}}(\text{COO}^-)$  were also seen. The  $^1\text{H-NMR}$  (DMSO- $d_6$ ) spectrum, Figure 1, revealed the presence of a carboxylic OH group at 12.84 ppm, aromatic proton signals in the range 8.62-78.20 ppm, and the methyl group at 2.44 ppm. Furthermore; the  $^{13}\text{C-NMR}$  spectra (Figure 1) displays the C-OH and  $\text{CH}_3$  at 192.34 and 21.64 ppm, respectively. Furthermore, the DEPT  $^{13}\text{C}$ - DEPT-135 confirm the proposed structure, Figure 1.

$^1\text{H-NMR}$ NADIA 20ANH  
proton\_su DMSO (C:\nmr-data) Student 7 $^{13}\text{C-NMR}$ NADIA 20ANH  
c13\_su DMSO (C:\nmr-data) Student 8

## DEPT-135 spectrum

NADIA 20ANH  
dept135\_su DMSO (C:\nmr\data) Student 8

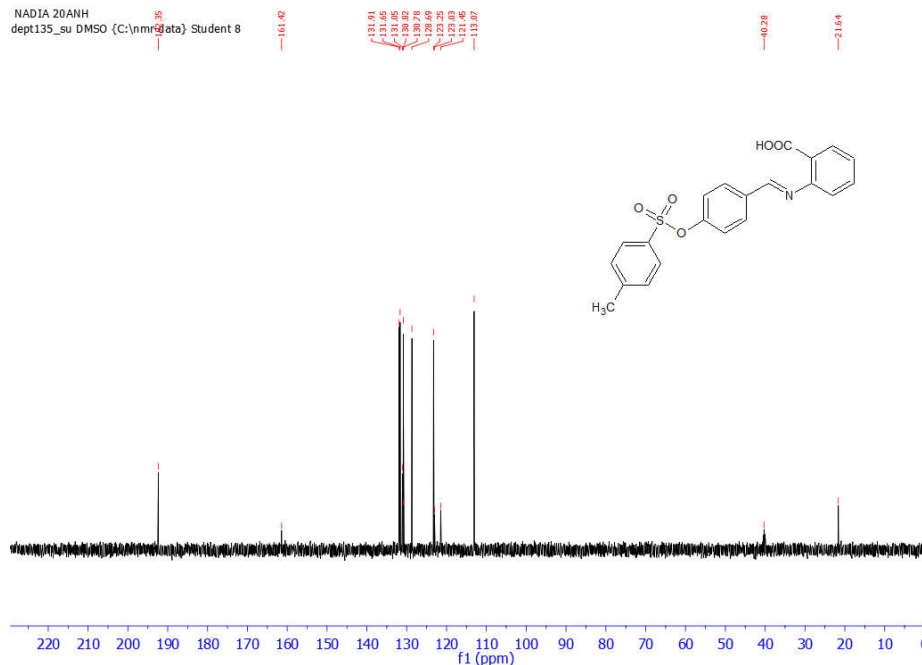


Figure 1.  $^1\text{H}$ -NMR,  $^{13}\text{C}$ -NMR and DEPT-135 spectrum of the free HL-ligand.

#### Structural characterization of the metal-ligand complexes

The complexes are almost completely soluble in DMF and DMSO at room temperature. Table 1 provides the analytical data and physicochemical properties for each molecule produced. Several techniques were used, including elemental analysis, Fourier transform infrared spectroscopy, molar conductivity, thermal analysis, magnetic susceptibility, and mass spectrometry, to provide a comprehensive account of the structure of HL ligand and its complexes. This outcome was the combined consequence of all of these approaches. Spectroscopic and analytical data was used to propose possible structures for the newly synthesized metal complexes (Scheme 1). Nonetheless, spectroscopic and analytical results corroborated the hypothesized frameworks. In addition, the data obtained from the elemental studies (C, H, and N) matched the expected structures.

#### Electronic spectra measurements

The following Table 1 displays the electronic absorption bands of the ligand and its metal complexes in DMF solutions. Figure 2 shows both the HL-ligand spectrum and the spectra of its metal complexes.

The bands seen at 315 and 370 nm for the unbound HL-ligand are the result of the  $\pi \rightarrow \pi^*$  and  $n \rightarrow \pi^*$  transitions. As a result of the fact that the electronic spectra of the Co(II) complex revealed two bands at 475 and 525 nm, an octahedral geometry was found to be the most likely explanation. The transitions  $^4\text{T}_{1g} \rightarrow ^4\text{A}_{2g}(\text{F})$  and  $^4\text{T}_{1g} \rightarrow ^4\text{T}_{2g}(\text{F})$ , respectively, were able to be assigned to these bands [28], Table 1.

Table 1. Physical properties, conductivity, UV-Vis, magnetic, and FT-IR results.

		HL ligand	Co(II) complex	Ni(II) complex	Cu(II) complex
Physical properties	Color	Pale pink	Brownish-red	Blue-violet	Yellowish-green
	Melting point (°C)	Pink	248-250	254-256	250-252
	Yield (%)	88	89	88	85
conductivity	$\mu_{\nu}$ , $\Omega^{-1}\text{cm}^2\text{mol}^{-1}$	--	9.85	8.99	9.07
	assignment	--	Non-electrolyte		
UV-Vis	$\lambda_{\text{max}}$ , nm	315, 370	475, 525	505, 640	495, 625
	$\mu_{\text{eff}}$ (B.M)	--	4.15	3.07	1.74
Magnetic	assignment	--	$d^7$ high spin ( $t_{2g}^5 e_g^2$ ) Octahedral	$d^8$ ( $e^4 t_2^4$ ) Tetrahedral	$d^9$ ( $t_{2g}^6 e_g^3$ ) Octahedral
	Stoichiometry	M : L	--	1 : 2	1 : 2
IR spectra	$\nu$ (-OH)	3322	3481	3475	3480
	$\nu$ (-CH=N)	1670	1589	1605	1615
	$\nu$ (-COO) <sub>asymmetric</sub>	1581	1605	1614	1610
	$\nu$ (-COO) <sub>symmetric</sub>	1424	1490	1485	1480
	$\nu$ (M-O)	--	578	580	577
	$\nu$ (M-N)	--	490	494	491
Elemental Analysis	C	63.97 (63.79)	54.47 (54.84)	57.33 (57.09)	53.70 (53.52)
	H	4.18 (4.33)	4.22 (4.38)	4.42 (4.11)	4.81 (4.49)
Found (calc.) %	N	3.41 (3.54)	3.31 (3.05)	3.55 (3.17)	2.48 (2.97)
	M	--	6.22 (6.41)	6.35 (6.64)	6.52 (6.74)

Two distinct bands could be seen in the electronic spectra of the Ni(II) complex, one at 505 nm and the other at 640 nm. These bands were able to be assigned to the  ${}^3A_{2g}(F) \rightarrow {}^3T_{2g}(P)$  transition and  ${}^3A_{2g}(F) \rightarrow {}^3T_{1g}(F)$  transition, respectively, both of which suggested a tetrahedral geometry around the Ni(II) centre [29], Table 1.

The d-d transition and the  ${}^2B_{1g} \rightarrow {}^2A_{1g}$  bands at 495 and 625 nm, respectively, in the electronic spectra of the Cu(II) complex may be explained by either a transition or a phonon resonant absorption. These transitions point to the existence of an octahedral geometry in the vicinity of the Cu(II) center, as shown in Table 1.

#### Complex stoichiometry

Figure 2 shows the results of a spectrophotometric Job's technique of continuous variation [30] experiment designed to calculate the metal-to-ligand molar ratio of the metal complexes. As expected from Job's law, maximum absorbance was seen at concentrations 0.65 times that of the ligand. Complexes of Co(II), Ni(II), and Cu(II) need a metal-to-ligand molar ratio of 1:2. (M:L).

#### FT-IR spectra

The distinctive vibration bands of the ligand and its metal complexes may be seen by studying the FT-IR spectra of the resulting compounds (in the range of 400–4000  $\text{cm}^{-1}$ ). Complex formation may affect bond strength, and IR spectroscopy can be used to probe atomic vibration at a certain stretching frequency. The IR spectrum line follows the motion of vibrational bands (Table 1). The HL ligand spectrum showed a band around 3322  $\text{cm}^{-1}$ , which is indicative of the stretching vibration of the -OH group. In the HL ligand, the absorption was prominent at 1670  $\text{cm}^{-1}$ , where

the (CH=N) was shown to be responsible. Additionally, the  $\nu(-\text{COO})_{\text{asymmetric}}$  frequency in the area of  $1581\text{ cm}^{-1}$  and  $\nu(-\text{COO})_{\text{symmetric}}$  frequency in the range of  $1424\text{ cm}^{-1}$  are seen in the spectra of HL-ligand, Table 1.

For metal ion coordination in metal complexes, the nitrogen atom of the azomethine group shifts the (-CH=N) band to lower frequencies ( $1589\text{-}1615\text{ cm}^{-1}$ ) [31, 32]. Metallic complexes showed elongation bands at  $1605\text{-}1614\text{ cm}^{-1}$  for  $\nu(-\text{COO})_{\text{asymmetric}}$  and at  $1480\text{-}1490\text{ cm}^{-1}$  for  $\nu(-\text{COO})_{\text{symmetric}}$ . Therefore, the oxygen atom in the carboxyl group must play a function in metal ion coordination. Using the azomethine group's nitrogen atom and the deprotonated carboxyl-oxygen, the HL-ligand forms a stable 6-membered chelate ring with the M(II) ions [33, 34]. In the spectra of metal-ligand complexes, there are two additional, weak bands seen at  $490\text{-}494\text{ cm}^{-1}$  and  $577\text{-}580\text{ cm}^{-1}$  [35], Table 1. The IR spectra of all the complexes matched with the elemental analyses, showing that the bandwidth at  $3475\text{-}3481\text{ cm}^{-1}$  is occupied by the (OH) stretching vibration of water molecules [36].

#### *Magnetic moment measurements*

The change in magnetization orientation caused by an external magnetic field is one way to approximate a material's magnetic susceptibility. Paramagnetic materials are those with unpaired electrons and positive susceptibilities, making them magnetically attractive. They also feature an extra uncoupled electron compared to typical atoms. Coordination chemists may learn about the three-dimensional structure of metal complexes by examining their magnetic susceptibility.

The  $d^8$  metal ion in the tetrahedral structure of the paramagnetic Ni(II) complex has an effective magnetic moment of 3.07 B.M., according to calculations.

In terms of magnetic susceptibility, complexes of cobalt(II) and copper(II) are both paramagnetic (4.15 and 1.74 B.M., respectively). The existence of three unpaired electrons is consistent with the reported value for the magnetic moment of the cobalt complex, which falls within the range typically seen for high-spin octahedral Co(II) complexes. The effective magnetic moment of 1.74 B.M. makes sense when considering the octahedral  $d^9$ -system implied by the Cu(II) complex.

#### *Microanalyses and molar conductance measurements*

In order to measure the molar conductance at room temperature, freshly prepared DMF solutions of the complexes were diluted to a concentration of  $1.0 \times 10^{-3}\text{ M}$  and tested. Results showing molar conductance values for the complexes in the range of  $9.07\text{-}9.99\text{ S.cm}^2\text{ mol}^{-1}$  provide further proof that the complexes do not possess an electrolytic feature.

#### *Thermal studies*

Differential thermal analysis and thermogravimetry (DTA/TG) were performed on metal complexes from ambient temperature to  $800\text{ }^\circ\text{C}$ . As was said in relation to the proposed formula for the compounds, mass loss occurs at each stage of the breakdown process. After the coordination water in the complexes degraded, the rest of the molecule followed suit. Figure 2 provide the DTA and TG properties of the relevant compounds, respectively.

Separate thermal breakdown processes occurred twice in the Co(II) complex,  $[\text{C}_{42}\text{H}_{40}\text{CoN}_2\text{O}_{14}\text{S}_2]$ . The initial breakdown takes place between  $30\text{ - }420\text{ }^\circ\text{C}$ , and it results in the loss of  $2\text{H}_2\text{O}_{\text{coord}} + 2\text{H}_2\text{O}_{\text{hyd}} + 2\text{C}_7\text{H}_7\text{SO}_3$  (calculated mass loss = 45.00%, experimental mass loss = 45.12%). The second phase, the breakdown of the remaining ligand fragments, is expected to account for a total mass loss of 46.69% at temperatures between  $420\text{ - }800\text{ }^\circ\text{C}$  (estimated mass loss = 46.85%), leaving behind just CoO as a metallic residue.

The breakdown of the Ni(II) complex  $[\text{C}_{42}\text{H}_{36}\text{N}_2\text{NiO}_{12}\text{S}_2]$  consists of two stages. At temperatures between  $30\text{ - }415\text{ }^\circ\text{C}$ , the mass of  $2\text{H}_2\text{O}_{\text{coord}} + 2\text{C}_7\text{H}_7\text{SO}_3$  decreases by 42.48%

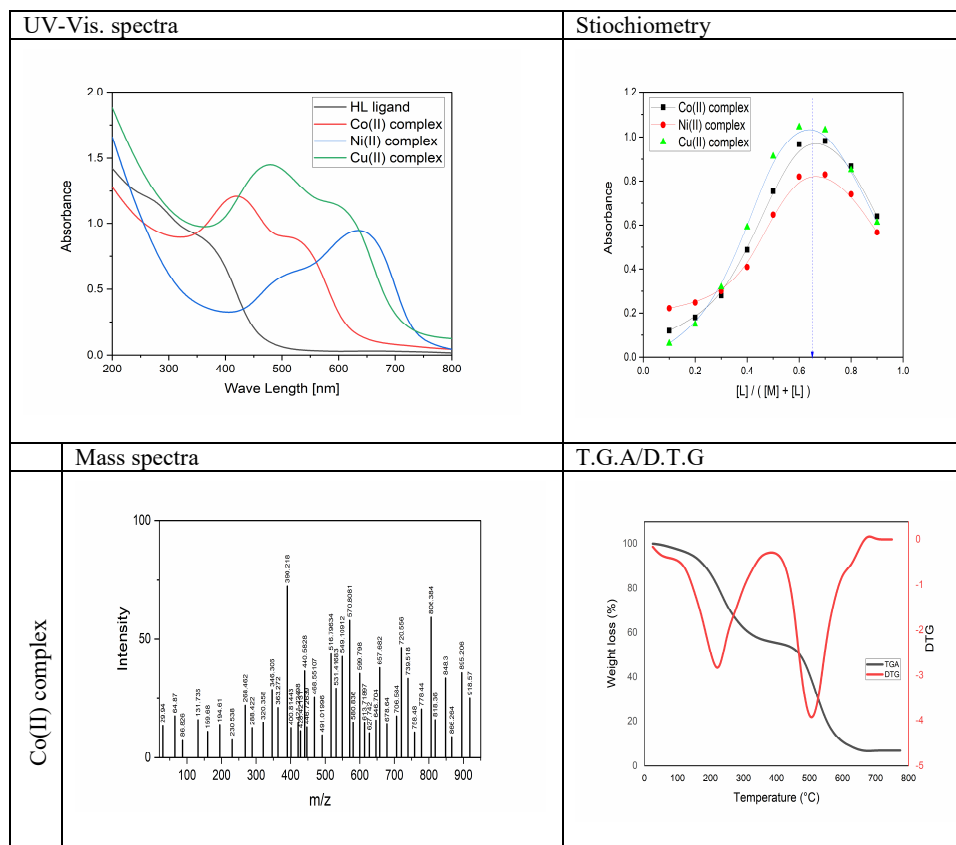
(calculated mass loss = 42.76%). Second, between 415 - 800 °C, the remaining ligand fragments dissolved, resulting in a total mass loss of 48.98% (calculated mass loss = 48.76%) and a metallic residue of NiO.

It was also demonstrated that the Cu(II) complex (with the formula  $[C_{42}H_{42}CuN_2O_{15}S_2]$ ) breaks down in two stages. The first stage included the loss of  $3H_2O_{coord} + 2H_2O_{hyd} + 2C_7H_7SO_3$  (estimated mass loss = 43.93%) at temperatures between 30 and 430 °C. Cu was determined to be the metallic remnant after the second phase, which occurred between 430 - 800 °C and resulted in an estimated total mass loss of 47.75% (mass loss = 47.64%).

The complexes' initial mass loss might have been caused by the hydration water and/or organic group. The presence of water molecules in the complexes has been confirmed by elemental analysis.

### Mass spectra

The mass spectrum is widely acknowledged as an important tool for describing structural features. The mass spectra of the given metal complexes were used to examine and compare the stoichiometric compositions of the compounds. Figure 2 depicts the mass spectra of the compounds under investigation. The molecular ion peaks ( $M^+$ ) in the mass spectra of the Co(II), Ni(II), and Cu(II) complexes at  $m/z$  918.57, 884.5, and 943.24, respectively, offer good corroboration of the calculated values of 920, 884.5, and 942.5.



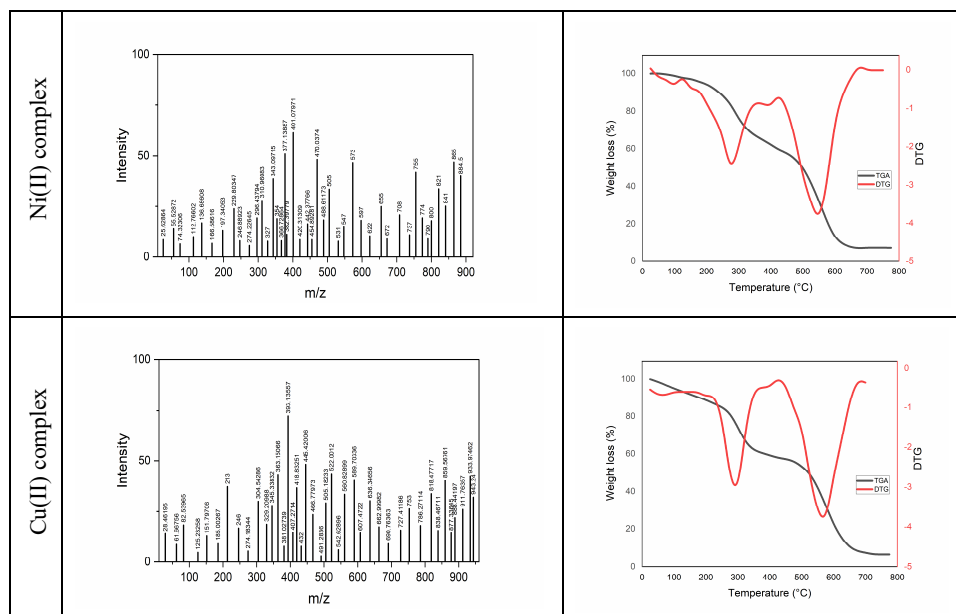
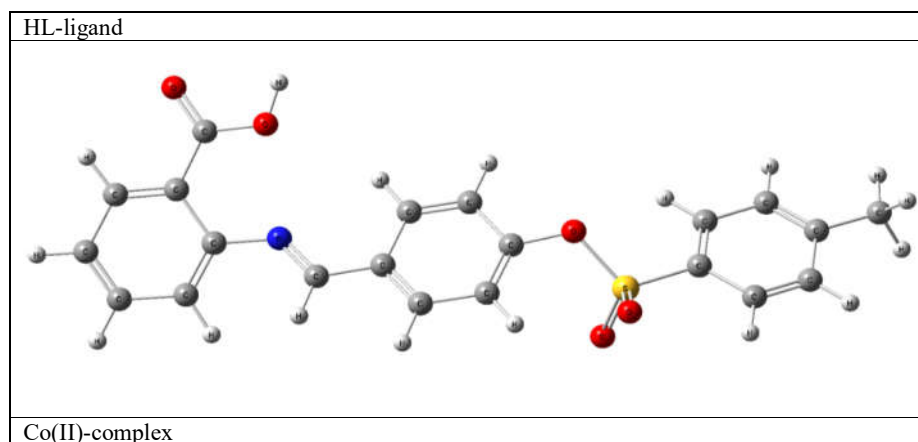


Figure 2. UV-Vis spectra, stoichiometry, mass spectra and tg graphs.

*DFT studies*

Molecular structures of the HL ligand and its metal complexes that have been optimized through the use of the DFT method are depicted in Figure 3.

HOMO and LUMO, Figure 4, also called frontier molecular orbitals, refer to the highest occupied and lowest unoccupied orbitals, respectively, in a given molecule (FMO). The kinetic stability and chemical reactivity of a molecule may be linked to its orbital energy gap ( $\Delta E$ ) [37, 38]. The border orbitals of highly polarizable, kinetically unstable molecules are packed closely together. The energy gap ( $\Delta E$ ) between the ground (HOMO) state and the most excited (LUMO) state of a ligand is often used as a proxy for the ligand's electronic structure.



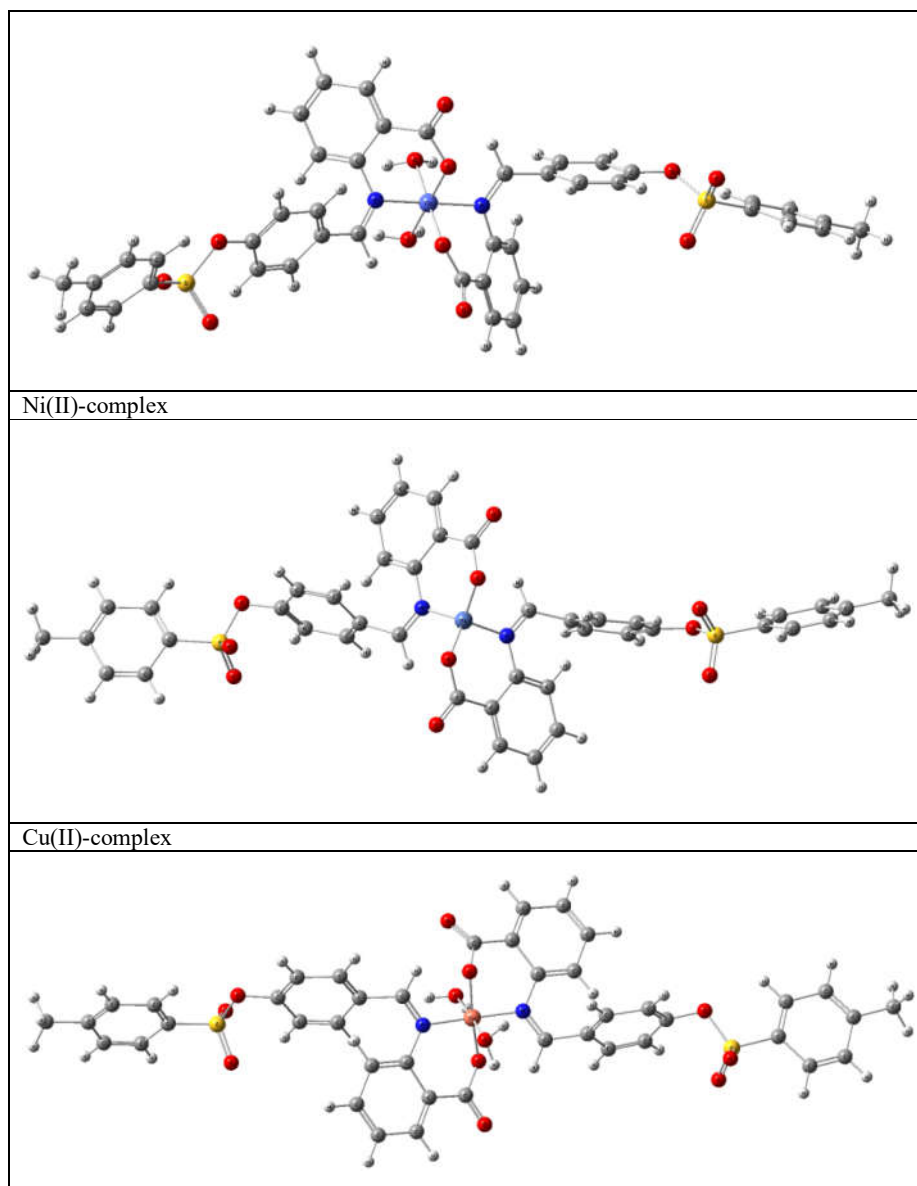
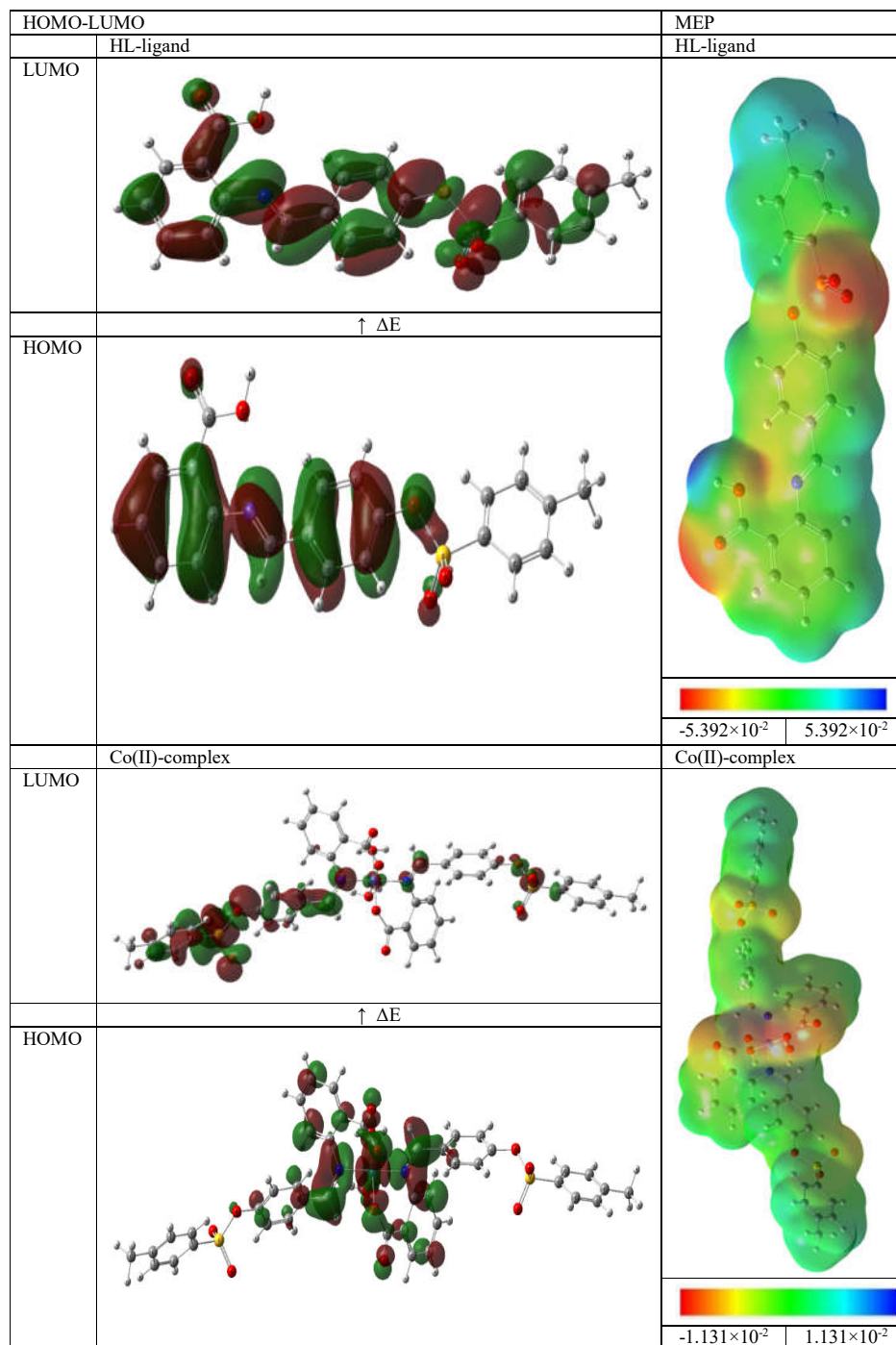


Figure 3. 3D geometries of the free ligand and its metal complexes.

Nevertheless, its impact on quantum chemistry remains significant [39]. Herein, we used density functional theory (DFT) with the B3LYP/6-311G(d, p) and LanL2dz basis sets to construct a three-dimensional model of the HOMO and LUMO states of the HL ligand and its metal complexes [40]. Table 2 displays the HOMO-LUMO gap energy determined for the HL ligand and its metal complexes (4.11, 1.96, 2.57, and 1.44).



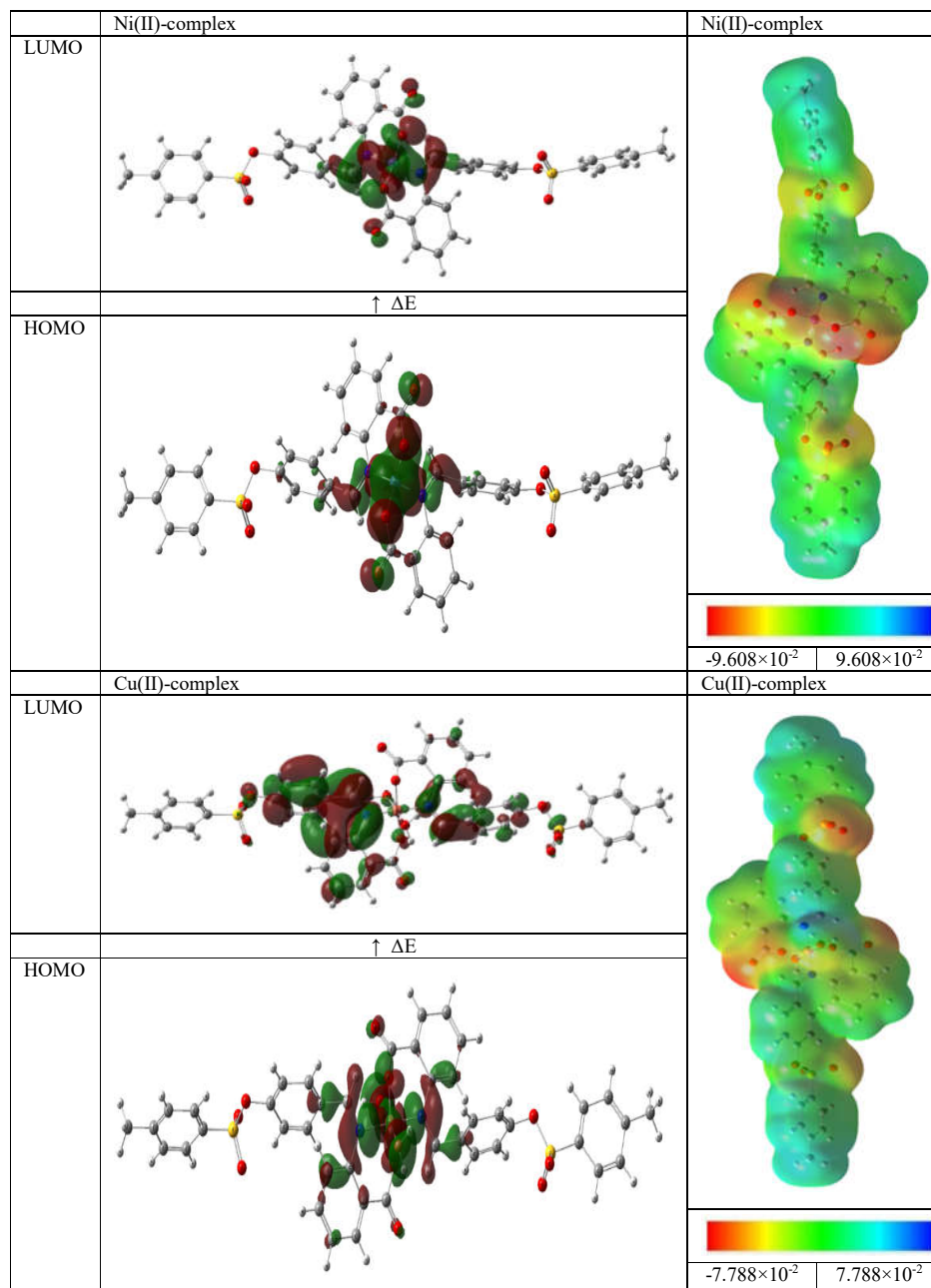


Figure 4. HOMO-LUMO, and MEP map.

The structural and conformational constraints of any sort of molecular system may be predicted by including  $\Delta E$ , a basic stability property, into theoretical models. To roughly assess a molecule's reactivity, the energy gap may be employed ( $\Delta E$ ). The equations in the scientific literature [41] that may be used to determine a substance's chemical hardness ( $\eta$ ), global softness ( $S$ ), global electrophilicity ( $\omega$ ), and absolute electronegativity ( $\chi$ ). The resultant quantum chemical parameter is listed in Table 2.

The capacity to classify substances as hard or soft is crucial for grading them, characterizing molecular reactivity using the HSAB rule (hard-soft-acid-base rule). This means that weak acids are drawn to weak bases, and strong acids to strong bases, when it comes to forming chemical bonds. Natural sources of strong acids and bases have been discovered as well. Examples of soft biological molecules include proteins, DNA, and other cellular building blocks. That's because soft molecules are more likely to interact with biological molecules than hard ones. As a result, softness promotes biological activity whereas hardness suppresses it [42]. Based on the available data, the reactivity ranking will be copper(II) complexes being the most stable, followed by cobalt(II), nickel(II), and the free ligand rank the complexes > cobalt(II) > nickel(II) >> the free ligand. The Table 2 clearly shows that when compared to the Co(II) complex, the Ni(II) complex, and the ligand, the Cu(II) complex is the superior option.

Table 2. Calculated chemical parameters.

	$E_{\text{HOMO}}$ (eV)	$E_{\text{LUMO}}$ (eV)	$\Delta E$ (eV)	I (eV)	A (eV)	$\chi$ (eV)	CP (eV)	$\eta$ (eV)	$\sigma$ (eV <sup>-1</sup> )	$\omega$ (eV)
Ligand	-6.33	-2.22	4.11	6.33	2.22	4.28	-4.28	2.05	0.24	4.45
Co(II) complex	-5.31	-3.35	1.96	5.31	3.35	4.33	-4.33	0.98	0.51	9.58
Ni(II) complex	-4.99	-2.42	2.57	4.99	2.42	3.71	-3.71	1.29	0.39	5.34
Cu(II) complex	-3.70	-2.25	1.44	3.70	2.25	2.97	-2.97	0.72	0.69	6.13

The sizes, shapes, and electrostatic potential values of molecules, as well as the distribution of their charges, are all shown in MEP diagrams. The picture makes it easy to see exactly where in the molecule nucleophilic and electrophilic processes take place. Red indicates an overabundance of electrons, whereas blue indicates an electrically weaker region of the molecule in MEP maps. MEP surface diagrams for the HL-ligand and its metal complexes were computed at the DFT/B3LYP/6-311G (d, p) and LanL2dz levels, Figure 4.

Studies of the MEP surfaces of the compounds that bore the names revealed that the oxygen and nitrogen atoms inside their structures had a negative charge density. The MEP had sway over this choice. The high charge density may have its origins in the high electronegativity of oxygen and nitrogen. According to MEP diagrams, this is where molecules are most likely to undergo a nucleophilic reaction. However, hydrogen atoms tend to occupy these electron-poor blue regions in isolated compounds. The surrounding oxygen and nitrogen atoms were far more electronegative than the atom itself, causing this effect. This happened because of this. Because electron-poor regions tend to cluster close to their targets, electrophilic reactions favor those regions where molecules come into contact.

#### *In vitro* antibacterial and antifungal activity screening

Studies of the HL ligand and its metal complexes against gram-positive (*S. aureus* (+ve) and *B. cereus* (+ve)) and gram-negative (*P. aeruginosa* (-ve) and *E. coli* (-ve)) bacteria and yeast (*A. flavus*, *T. rubrum*, *C. albicans*) were conducted using the disc diffusion method in DMSO solvent, Table 3. Inhibitory values against these bacteria and fungi as described in the literature are shown in Table 3. The antibiotic drug chloramphenicol was used in a positive control screening for fungi and bacteria. We used both the free ligand and the metal complexes of the ligand as a basis for our comparisons. Confirming their inhibitory capability is the finding that the generated

complexes exhibit higher antibacterial/antifungal activity than the free ligand against all species (Table 3). In place of the common antibiotic chloramphenicol, these metal complexes function admirably. It was found that the complex of Cu(II) was very efficient against even the most resistant bacteria and molds. In addition, the Co(II) complex had the second largest inhibition gradients.

Table 3. The anti-bacterial and anti-fungal activity of the titled compounds in terms of inhibition zone (IZ, mm), and activity index (%).

Anti-bacterial activity						
bacterial strains		Ligand	Co complex	Ni complex	Cu complex	Chloramphenicol
<i>P. aeruginosa</i> (-ve)	IZ	8	16	16	16	18
	%	44.44	88.89	88.89	88.89	
	MIC	50	12.5	6.25	6.25	
<i>E. coli</i> (-ve)	IZ	9	16	18	18	20
	%	45.00	80.00	90.00	90.00	
	MIC	25	6.25	6.25	6.25	
<i>S. aureus</i> (+ve)	IZ	9	15	14	16	18
	%	50.00	83.33	77.78	88.89	
	MIC	25	12.5	6.25	6.25	
<i>B. cereus</i> (+ve)	IZ	8	15	14	15	18
	%	44.44	83.33	77.78	83.33	
	MIC	50	6.25	6.25	6.25	
Anti-fungal activity						
fungal strains		Ligand	Co complex	Ni complex	Cu complex	Chloramphenicol
<i>A. flavus</i>	IZ	9	16	16	17	19
	%	47.37	84.21	84.21	89.47	
	MIC	25	12.5	6.25	6.25	
<i>T. rubrum</i>	IZ	9	18	17	18	22
	%	40.91	81.82	77.27	81.82	
	MIC	50	12.5	6.25	12.5	
<i>C. albicans</i>	IZ	9	17	16	17	21
	%	42.86	80.95	76.19	80.95	
	MIC	50	12.5	6.25	6.25	

The activity of the complex is higher than that of the free ligand. Perhaps the concept of chelation might shed some light on this observation. It was found that the polarity of metal complexes was greatly diminished as a result of the interaction between ligand ions and metal ions. In order to share electrons with ligands, metal ions must first donate some of their own positive charge, and their orbitals may overlap with those of the ligands [43]. To do this, the lipophilicity of metal complexes is increased by promoting the delocalization of pi electrons inside the chelate ring. Metal complexes may penetrate deeper through the lipid membrane and reduce bacterial populations due to their increased lipophilicity. It's possible that these metal complexes impede cellular respiration, preventing the production of "proteins" that would otherwise limit the organism's capacity for future development.

To further assess the *in vitro* antimicrobial and antifungal activity of each chemical, we determined the minimum inhibitory concentration (MIC) of each compound against our test bacteria and fungi. The MIC of an antimicrobial or antifungal agent is the lowest concentration at which the growth of microorganisms is visibly inhibited. In Table 3, we present the compounds investigated, the bacteria and fungi used as test subjects, and the MICs for each component. Based on the data in Table 3, the activity index (%) of the aforementioned compounds ranged from 40 to 50% for free ligand and increased to 70 to 90% for metal complexes.

*Molecular docking studies*

Table 4. Molecular docking findings of the prepared materials.

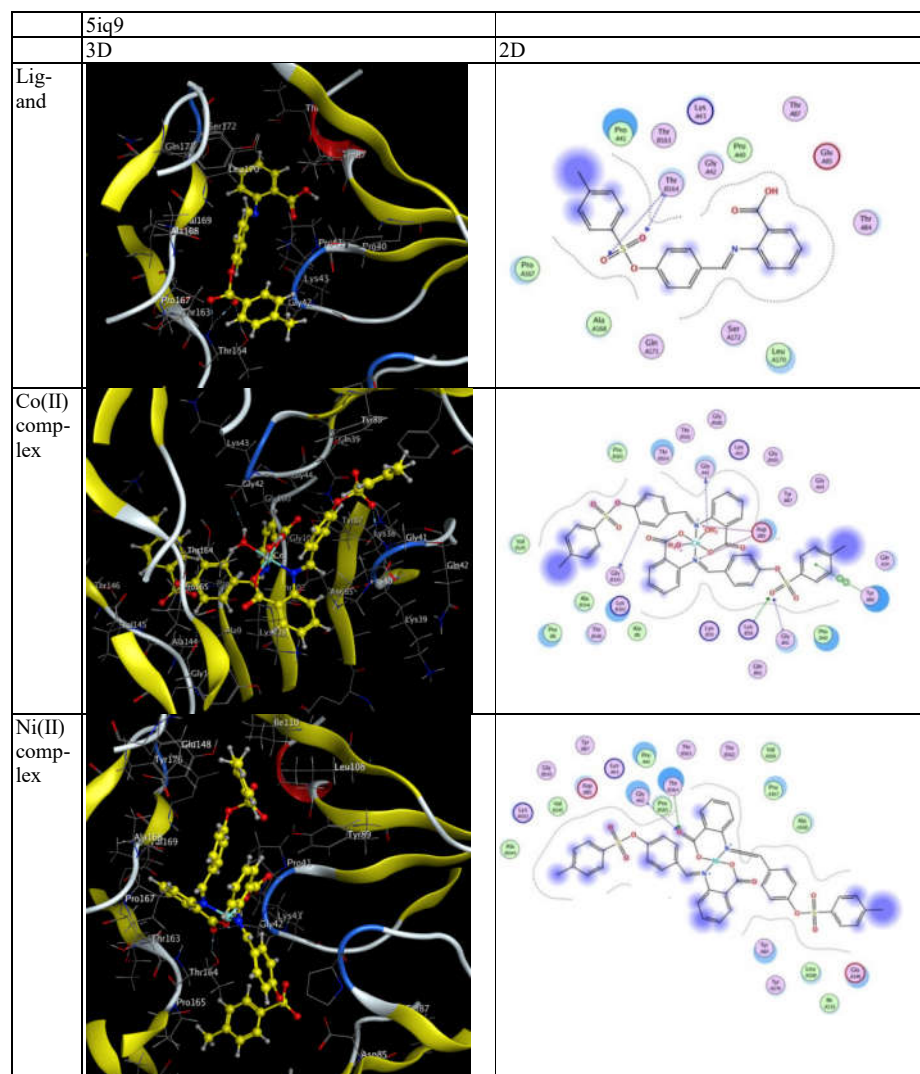
	5iq9					
	Ligand	Receptor	Interaction	Distance	E (kcal/mol)	S (kcal/mol)
Ligand	O 1	THR 164	H.A	3.23	-1.70	-6.51
	O 21	THR 164	H.A	3.11	-2.40	
	O 21	THR 164	H.A	2.90	-1.50	
Co(II) complex	C 17	GLY 143	H.A	3.31	-0.70	-7.79
	O 90	GLY 42	H.A	3.34	-1.20	
	O 65	LYS 38	H.A	2.89	-7.10	
	O 65	GLY 41	H.A	3.24	-1.80	
	N 4	ASP 85	I	2.95	-4.90	
	N 48	ASP 85	I	2.86	-5.50	
	6-ring	TYR 89	pi-pi	3.91	-0.13	
Ni(II) complex	O 11	GLY 42	H.A	3.17	-0.80	-7.58
	O 11	THR 164	H.A	2.60	-0.50	
Cu(II) complex	C 16	GLY 100	H.A	3.27	-0.70	-8.38
	O 93	GLY 42	H.A	3.01	-6.00	
	O 93	THR 164	H.A	2.69	-7.30	
	N 48	ASP 85	I	3.54	-1.70	
	6-ring	GLY 42	pi-H	3.56	-0.60	
	Ligand	Receptor	Interaction	Distance	E (kcal/mol)	Receptor
	6clv					
Ligand	O 12	ASP 42	H.A	2.87	-6.50	-7.03
	O 1	TYR 212	H.A	2.83	-2.10	
Co(II) complex	C 17	MET 37	H.A	3.52	-1.00	-7.98
	O 21	MET 37	H.A	2.89	-0.970	
	O 90	ALA 41	H.A	3.02	-2.60	
	O 90	ASP 42	H.A	2.54	-10.50	
	O 93	MET 37	H.A	2.92	-2.50	
	O 1	ARG 176	H.A	3.11	-0.80	
	O 1	ARG 176	H.A	2.68	-3.30	
	O 21	ASP 78	H.A	3.17	-0.70	
	N 4	ASP 42	I	3.25	-3.00	
	O 90	ASP 42	I	2.54	-8.40	
Ni(II) complex	C 47	LYS 34	H.A	3.39	-0.90	-7.39
	N 48	ASP 38	I	2.72	-6.70	
	N 48	ASP 38	I	3.20	-3.30	
Cu(II) complex	O 90	GLY 40	H.A	2.53	-4.10	-8.46
	O 90	ASP 42	H.A	2.96	-3.40	
	O 93	ALA 41	H.A	2.79	-3.20	
	O 93	ASP 42	H.A	3.04	-3.50	
	O 11	LYS 3	H.A	3.43	-1.30	
	O 21	ARG 176	H.A	2.82	-3.30	
	O 90	ASP 42	I	2.96	-4.80	
O 93	ASP 42	I	3.04	-4.20		

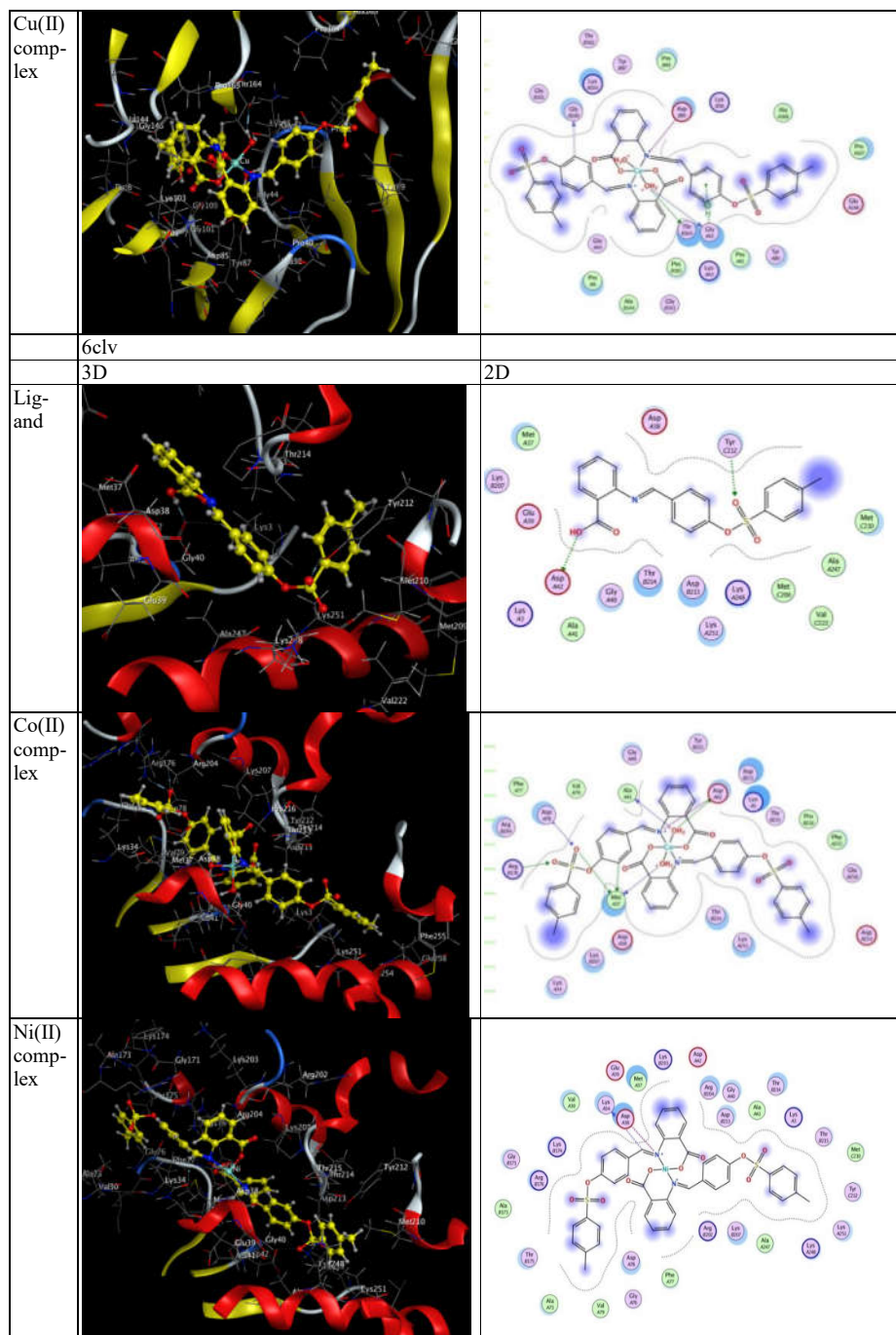
H.D = H-donor, H.A = H-acceptor, I = ionic

The synthesized compounds were tested for efficacy against bacteria by docking with the target protein [44, 45]. The purpose of the experiment was to see whether the inhibitors' binding attractiveness correlated with their *in vitro* antibacterial activity. Researchers utilizing molecular docking may use virtual compound screening and scoring algorithms to predict which compounds

have the greatest binding affinities [46]. This means that we may be able to focus on the molecules that are most suited to form a bind with our target. Molecules participating in an interaction are represented as pieces of a jigsaw puzzle to facilitate a holistic, three-dimensional understanding of events like the active site binding of a target receptor and a substrate.

These synthetic materials serve as an analogue substrate for the protein receptor seen in two crystal structures of DHPS bound to pterin-sulfonamide conjugates [47] (PDB ID 5JQ9 and 6CLV, respectively, from *E. coli* and *S. aureus*). The docking findings for the compounds under study are summarized in Table 4, and the proper orientation of the molecules inside the binding pocket is shown in Figure 5.





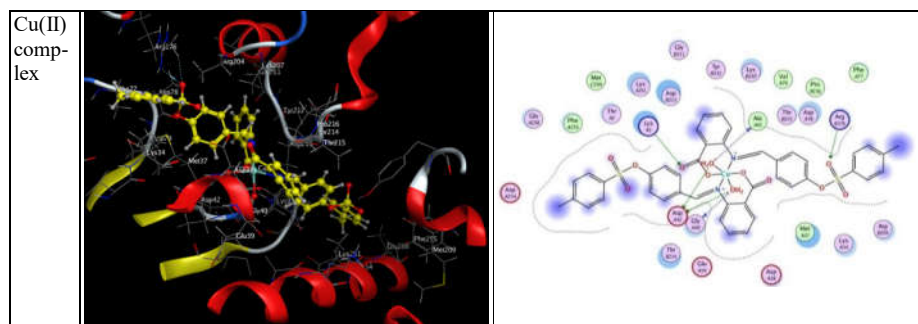


Figure 5. 3D and 2D orientation of the substrate-protein complex.

According to docking experiments, the estimated binding energies of the compounds with *E. coli* DHPS (5JQ9) were somewhat higher than those with *S. aureus* DHPS (6CLV). Evidence like this point refers to DHPS inhibition as the probable culprit in *E. coli*. The binding process is spontaneous, and the compounds may be employed as a therapy, however, all of the compounds examined exhibited negative projected binding energies (Table 4).

As demonstrated in Figure 5 and Table 4, docking to the active pocket of the target receptor necessitates a high number of hydrogen bonds, hydrophobic interactions, and negative docking scores (S). Activation of the receptor is shown as a result of the docked substrates interacting with the active site. Docking energies (also known as binding energies) are expected to be larger for metal complexes than for their parent ligands, according to computational modeling. Metal complexes are more responsive than their parent ligands, as has been shown by several biological studies. Due to these modifications to the parent ligands, potent new antibacterial agents have been identified. After trying other receptors, Cu(II) complex emerged as the clear victor.

### CONCLUSION

New 2-[(4-[(4-methylphenyl)sulfonyl]methylene)aminobenzoic acid ligand-Co(II), Ni(II), and Cu(II) complexes are synthesized and characterized. Quantum chemical calculations, based on DFT/B3LYP with 6-311G (d,p) and LANL2DZ, revealed a tetrahedral geometry for the Co(II) complex and octahedral geometry for the Ni(II) and Cu(II) complexes. The HOMO-LUMO gap tests indicated that the Cu(II) complex was the most reactive and least stable of the newly synthesized compounds. The newly synthesized compounds were also examined *in vitro* for their antibacterial and antifungal properties. Molecular docking was used to learn more about how the synthesized chemicals bound to the 5JQ9 and 6CLV proteins. Molecular docking simulations' results corroborated those of *in vitro* antibacterial efficacy tests. Binding energy was the lowest for the Cu(II) complex (-8.46 and -8.38 kcal/mol), out of all the compounds tested. In light of these findings, the Cu(II) complex merits more investigation as a potential antibacterial and antifungal agent.

### ACKNOWLEDGMENT

The authors extend their appreciation to the Deanship of Scientific Research at Jouf University for funding this work through research grant No (697/ 39).

### REFERENCES

1. Dalia, S.A.; Afsan, F.; Hossain, M.S.; Khan, M.N.; Zakaria, C.; Zahan, M.E.; Ali, M. A short review on chemistry of Schiff base metal complexes and their catalytic application. *Int. J. Chem. Stud.* **2018**, *6*, 2859-2867.

2. Mohapatra, R.K.; Sarangi, A.K.; Azam, M.; El-ajaily, M.M.; Kudrat-E-Zahan, M.; Patjoshi, S.B.; Dash, D.C. Synthesis, structural investigations, DFT, molecular docking and antifungal studies of transition metal complexes with benzothiazole based Schiff base ligands. *J. Mol. Struct.* **2019**, *1179*, 65-75.
3. Khan, E.; Hanif, M.; Akhtar, M.S. Schiff bases and their metal complexes with biologically compatible metal ions; biological importance, recent trends and future hopes. *Rev. Inorg. Chem.* **2022**, *42*, 307-325.
4. Ebosie, N.P.; Ogwuegbu, M.O.; Onyedika, G.O.; Onwumere, F.C. Biological and analytical applications of Schiff base metal complexes derived from salicylidene-4-aminoantipyrine and its derivatives: A review. *J. Iran. Chem. Soc.* **2021**, *18*, 3145-3175.
5. Abdel-Kader, N.S.; Moustafa, H.; El-Ansary, A.L.; Sherif, O.E.; Farghaly, A.M. A coumarin Schiff base and its Ag(I) and Cu(II) complexes: Synthesis, characterization, DFT calculations and biological applications. *New J. Chem.* **2021**, *45*, 7714-7730.
6. Abdel-Monem, R.A.; Khalil, A.M.; Darwesh, O.M.; Hashim, A.I.; Rabie, S.T. Antibacterial properties of carboxymethyl chitosan Schiff-base nanocomposites loaded with silver nanoparticles. *J. Macromol. Sci. Part A* **2020**, *57*, 145-155.
7. Hasan, M.R.; Hossain, M.A.; Salam, M.A.; Uddin, M.N. Nickel complexes of Schiff bases derived from mono/diketone with anthranilic acid: Synthesis, characterization and microbial evaluation. *J. Taibah Univ. Sci.* **2016**, *10*, 766-773.
8. El-Saghier, A.M.; Abosella, L.; Aborahma, G.A.; Elakesh, E.O.; Abdelhamid, A.A.; Gad, M. A. Synthesis and insecticide evaluation of some new oxopropylthiourea compounds as insect growth regulators against the cotton leafworm, *Spodoptera littoralis*. *Sci. Rep.* **2023**, *13*, 13089.
9. Abd El-Lateef, H.M.; Khalaf, M.M.; Gouda, M.; Kandeel, M.; Amer, A.A.; Abdelhamid, A.A.; Drar, A.M.; Gad, M.A. Functionalized pyridines: Synthesis and toxicity evaluation of potential insecticidal agents against *Aphis craccivora*. *ACS Omega* **2023**, *8*, 29685-29692.
10. Elkanzi, N.A.; Al-Hazmi, A.K.G.; Bakr, R.B.; Gad, M.A.; Abd El-Lateef, H.M.; Ali, A.M. Design and synthesis of pyridine and thiazole derivatives as eco - friendly insecticidal to control olive pests. *Chem. Biodivers.* **2023**, *20*, e202300559.
11. Ali, A.M.; Salah, H.; Gad, M.A.; Youssef, M.A.M.; Elkanzi, N.A.A. Design, synthesis, and SAR studies of some novel chalcone derivatives for potential insecticidal bioefficacy screening on *Spodoptera frugiperda* (Lepidoptera: Noctuidae). *ACS Omega*, **2022**, *7*, 40091-40097.
12. Oelkers, B.; Sundermeyer, J. Sulfonate-tagged 1,4-diazabutadiene (DAD S) ligands and their noble-metal complexes—synthesis, characterization and immobilization in ionic liquids. *Dalton Trans.* **2011**, *40*, 12727-12741.
13. Bakry, M.; Mohammed, L.; Dabour, N.; Gad, M. Design and synthesis of novel N,N'-substituted benzamide derivatives as potential insecticidal agents against the white mango scale insect, *Aulacaspis tubercularis* (Hemiptera: Diaspididae). *Curr. Chem. Lett.* **2024**, *13*, 173-186.
14. Tomberg, A. Gaussian 09W Tutorial, an Introduction to Computational Chemistry Using G09W and Avogadro Software, **2013**, 1-34.
15. Becke, A.D. Density-functional exchange-energy approximation with correct asymptotic behavior. *Phys. Rev. A* **1988**, *38*, 3098.
16. Abd El-Lateef, H.M.; Khalaf, M.M.; Kandeel, M.; Abdou, A. Synthesis, characterization, DFT, biological and molecular docking of mixed ligand complexes of Ni(II), Co(II), and Cu(II) based on ciprofloxacin and 2-(1H-benzimidazol-2-yl) phenol. *Inorg. Chem. Commun.* **2023**, *155*, 111087.
17. Ghobadi, H.; Ghiasi, R.; Jamehbozorgi, S. Effect of the external electric field on the electronic structure and aromaticity of iridabenzene: A DFT study. *J. Struct. Chem.* **2019**, *60*, 547-555.

18. Mohapatra, R.K.; Mahal, A.; Ansari, A.; Kumar, M.; Guru, J.P.; Sarangi, A.K.; Abdou, A.; Mishra, S.; Aljeldah, M.; AlShehail, B.M.; Alissa, M. Comparison of the binding energies of approved mpox drugs and phytochemicals through molecular docking, molecular dynamics simulation, and ADMET studies: An in silico approach. *J. Biosaf. Biosecurity* **2023**, *5*, 118-132.
19. Hay, P.J.; Wadt, W.R.; Ab initio effective core potentials for molecular calculations. Potentials for the transition metal atoms Sc to Hg. *J. Chem. Phys.*, **1985**, *82*, 270-283.
20. Balouiri, M.; Sadiki, M.; Ibnsouda, S.K. Methods for *in vitro* evaluating antimicrobial activity: A review. *J Pharm Anal.* **2016**, *6*, 71-79.
21. Singh, V.P.; Katiyar, A. Synthesis, spectral characterization and antimicrobial activity of some transition metal(II) complexes with acetone *p*-amino acetophenone benzoylhydrazone. *Pestic. Biochem. Physiol.* **2008**, *92*, 8-14.
22. Hrichi, H.; Elkanzi, N.A.; Ali, A.M.; Abdou, A. A novel colorimetric chemosensor based on 2-[(carbamothioylhydrazono) methyl] phenyl 4-methylbenzenesulfonate (CHMPMBS) for the detection of Cu(II) in aqueous medium. *Res. Chem. Intermed.* **2023**, *49*, 2257-2276.
23. Shaaban, S.; Abdou, A.; Alhamzani, A.G.; Abou-Krishna, M.M.; Al-Qudah, M.A.; Alaasar, M.; Youssef, I.; Youssef, T.A. Synthesis and in silico investigation of organoselenium-clubbed Schiff bases as potential Mpro inhibitors for the SARS-CoV-2 replication. *Life* **2023**, *13*, 912.
24. Hammoudeh, D.I.; Zhao, Y.; White, S.W.; Lee, R.E. Replacing sulfa drugs with novel DHPS inhibitors. *Future Med. Chem.* **2013**, *5*, 1331-1340.
25. Yun M-K.; Yinan Wu.; Li Z.; Ying Zhao M.; Waddell B.; Ferreira, AM.; Lee RE.; Bashford, D.; White, S.W. Catalysis and sulfa drug resistance in dihydropteroate synthase. *Science* **2012**, *335*, 1110-1114.
26. Zhao, Y.; Shadrack, W.R.; Wallace, M.J.; Yinan, Wu.; Griffith, E.C.; Qi, J.; Yun, M.-K.; White S.W. Lee, R.E. Pterin-sulfa conjugates as dihydropteroate synthase inhibitors and antibacterial agents. *Bioorg. Med. Chem. Lett.* **2016**, *26*, 3950-3954.
27. El-Saghier, A.M.; Abdou, A.; Mohamed, M.A.; Abd El-Lateef, H.M.; Kadry, A.M. Novel 2-acetamido-2-ylidene-4-imidazole derivatives (El-Saghier reaction): Green synthesis, biological assessment, and molecular docking. *ACS Omega* **2023**, *8*, 30519-30531.
28. Jabbar, A.I.; Al-jibouri, M.N.; Ismail, A.H. Synthesis and structural studies of transition metals complexes with poly dentate azo dye ligand derived from coumarine. *Egypt. J. Chem.* **2021**, *64*, 6481-6485.
29. Saeed, I.A. Synthesis and characterization of ligating properties of organic disulfides complexes with Co, Ni and Cu metal ions. *Tikrit J. Pure Sci.* **2012**, *17*, 2.
30. Job, P. Formation and stability of inorganic complexes in solution. *Ann. Chim.* **1928**, *9*, 113-134.
31. Al-Ayash, S.R.; Al-Noor, T.H.; Abdou, A. Synthesis and characterization of metals complexes with uracil and uracil derivatives (a review). *Russ. J. Gen. Chem.* **2023**, *93*, 987-995.
32. El-Saghier, A.M.; Enaili, S.S.; Kadry, A.M.; Abdou, A.; Gad, M.A. Green synthesis, biological and molecular docking of some novel sulfonamide thiadiazole derivatives as potential insecticidal against *Spodoptera littoralis*. *Sci. Rep.* **2023**, *13*, 19142-19142.
33. Latif, M.A.; Ahmed, T.; Hossain, M.S.; Chaki, B.M.; Abdou, A.; Kudrat-E-Zahan, M. Synthesis, spectroscopic characterization, DFT calculations, antibacterial activity, and molecular docking analysis of Ni(II), Zn(II), Sb(III), and U(VI) metal complexes derived from a nitrogen-sulfur Schiff base. *Russ. J. Gen. Chem.* **2023**, *93*, 389-397.
34. Jarad, A.J.; Dahi, M.A.; Al-Noor, T.H.; El-ajaily, M.M.; AL-Ayash, S.R.; Abdou, A. Synthesis, spectral studies, DFT, biological evaluation, molecular docking and dyeing performance of 1-(4-((2-amino-5-methoxy) diazenyl) phenyl) ethanone complexes with some metallic ions. *J. Mol. Struct.* **2023**, *1287*, 135703.
35. Abd El-Lateef, H.M.; Khalaf, M.M.; Kandeel, M.; Amer, A.A.; Abdelhamid, A.A.; Abdou, A. New mixed-ligand thioether-quinoline complexes of nickel(II), cobalt(II), and copper(II):

- Synthesis, structural elucidation, density functional theory, antimicrobial activity, and molecular docking exploration. *Appl. Organomet. Chem.* **2023**, 37, e7134.
36. Abu-Dief, A.M.; El-Khatib, R.M.; El-Dabea, T.; Abdou, A.; Aljohani, F.S.; Al-Farraj, E.S.; Barnawi, I.O.; Ali, M.A.E.A.A. Fabrication, structural elucidation of some new metal chelates based on N-(1H-Benzoimidazol-2-yl)-guanidine ligand: DNA interaction, pharmaceutical studies and molecular docking approach. *J. Mol. Liq.* **2023**, 386, 122353.
  37. Abd El-Lateef, H.M.; Khalaf, M.M.; Kandeel, M.; Amer, A.A.; Abdelhamid, A.A.; Abdou, A. Designing, characterization, biological, DFT, and molecular docking analysis for new FeAZD, NiAZD, and CuAZD complexes incorporating 1-(2-hydroxyphenylazo)-2-naphthol (H2AZD). *Comput. Biol. Chem.* **2023**, 105, 107908.
  38. Shokr, E.K.; Kamel, M.S.; Abdel-Ghany, H.; Ali, M.A.E.A.A.; Abdou, A. Synthesis, characterization, and DFT study of linear and non-linear optical properties of some novel thienothiophene azo dye derivatives. *Mater. Chem. Phys.* **2022**, 290, 126646.
  39. Murugan, T.; Venkatesh, R.; Geetha, K.; Abdou, A. Synthesis, spectral investigation, DFT, antibacterial, antifungal and molecular docking studies of Ni(II), Zn(II), Cd(II) complexes of tetradentate schiff-base ligand. *Asian J. Chem.* **2023**, 35, 1509-1517.
  40. Abdou, A.; Omran, O.A.; Al-Fahemi, J.H.; Jassas, R.S.; Al-Rooqi, M.M.; Hussein, E.M.; Moussa, Z.; Ahmed, S.A. Lower rim thiacalixarenes derivatives incorporating multiple coordinating carbonyl groups: Synthesis, characterization, ion-responsive ability and DFT computational analysis. *J. Mol. Struct.* **2023**, 1293, 136264.
  41. Ali, M.A.E.A.A.; Elhady, O.; Abdou, A.; Alhashmialameer, D.; Eskander, T.N.A.; Abu-Dief, A.M. Development of new 2-(benzothiazol-2-ylimino)-2,3-dihydro-1H-imidazol-4-ol complexes as a robust catalysts for synthesis of thiazole 6-carbonitrile derivatives supported by DFT studies. *J. Mol. Struct.* **2023**, 1292, 136188.
  42. Najar, A.M.; Eswayah, A.; Moftah, M.B.; Omar, M.K.R.; Bobtaina, E.; Najwa, M.; Elhisadi, T.A.; Tahani, A.; Tawati, S.M.; Khalifa, A.M.M.; Abdou, A.; Emhamed DowAltome, A. Rigidity and flexibility of pyrazole, s-triazole, and v-triazole derivative of chloroquine as potential therapeutic against COVID-19. *J. Med. Chem. Sci.* **2023**, 6, 2056-2084.
  43. Hossain, M.S.; Khushy, K.A.; Latif, M.A.; Hossen, M.F.; Asraf, M.A.; Kudrat-E-Zahan, M.; Abdou, A.; Co(II), Ni(II), and Cu(II) complexes containing isatin-based Schiff base ligand: Synthesis, physicochemical characterization, DFT calculations, antibacterial activity, and molecular docking analysis. *Russ. J. Gen. Chem.* **2022**, 92, 2723-2733.
  44. Abd El-Lateef, H.M.; Khalaf, M.M.; Amer, A.A.; Kandeel, M.; Abdelhamid, A.A.; Abdou, A. Synthesis, characterization, antimicrobial, density functional theory, and molecular docking studies of novel Mn(II), Fe(III), and Cr(III) complexes incorporating 4-(2-hydroxyphenyl azo)-1-naphthol (Az). *ACS Omega* **2023**, 8, 25877-25891.
  45. Shaaban, S.; Al-Faiyz, Y.S.; Alsulaim, G.M.; Alaasar, M.; Amri, N.; Ba-Ghazal, H.; Al-Karmalawy, A.A.; Abdou, A. Synthesis of new organoselenium-based succinilic and maleanilic derivatives and in silico studies as possible SARS-CoV-2 main protease inhibitors. *Inorganics* **2023**, 11, 321.
  46. Abd El-Lateef, H.M.; Khalaf, M.M.; Heikal, F.E.T.; Abdou, A. Fe(III), Ni(II), and Cu(II)-moxifloxacin-tri-substituted imidazole mixed ligand complexes: Synthesis, structural, DFT, biological, and protein-binding analysis. *Inorg. Chem. Commun.* **2023**, 158, 111486.
  47. El-Remaily, M.A.E.A.A.A.; El-Dabea, T.; El-Khatib, R.M.; Abdou, A.; El Hamd, M.A.; Abu-Dief, A.M. Efficiency and development of guanidine chelate catalysts for rapid and green synthesis of 7-amino-4,5-dihydro-tetrazolo [1,5-a] pyrimidine-6-carbonitrile derivatives supported by density functional theory (DFT) studies. *Appl. Organomet. Chem.* **2023**, 37, e72.